

Effective hydrodynamic hydrogen escape from an early Earth atmosphere inferred from high-accuracy numerical simulation

Kiyoshi Kuramoto^{a,b,*}, Takafumi Umemoto^{a,c}, Masaki Ishiwatari^{a,b}

^a*Department of CosmoSciences, Hokkaido University, Sapporo 060-0810, Japan*

^b*Center for Planetary Sciences, Kobe 650-4407, Japan*

^c*Nihon Unisys, Tokyo 650-4407, Japan*

Abstract

Hydrodynamic escape of hydrogen driven by solar extreme ultraviolet (EUV) radiation heating is numerically simulated by using the constrained interpolation profile scheme, a high-accuracy scheme for solving the one-dimensional advection equation. For a wide range of hydrogen number densities at the lower boundary and solar EUV fluxes, more than half of EUV heating energy is converted to the mechanical energy of the escaping hydrogen. Less energy is lost by downward thermal conduction even giving low temperature for the atmospheric base. This result differs from a previous numerical simulation study that yielded much lower escape rates by employing another scheme in which relatively strong numerical diffusion is implemented. Because the solar EUV heating effectively induces hydrogen escape, the hydrogen mixing ratio was likely to have remained lower than 1 vol% in the anoxic Earth atmosphere during the Archean era.

*Department of CosmoSciences, Hokkaido University, Kita 10 Nishi 8, Kita-ku, Sapporo 060-0810, Japan. Phone +81-11-706-3827, Fax +81-11-706-2760

Email address: keikei@ep.sci.hokudai.ac.jp (Kiyoshi Kuramoto)

Keywords: early earth, hydrodynamic escape, hydrogen, atmospheric composition, solar radiation

1. Introduction

The hydrodynamic escape of hydrogen driven by solar extreme ultraviolet (EUV) flux is a key process for controlling the evolution of the early Earth atmosphere and surface environment. For an atmosphere having a hydrogen-dominated upper layer, it was suggested that EUV heating energy is effectively transferred to mechanical energy of the outflow gas (e.g., Sekiya et al., 1980; Watson et al., 1981). Such effective escape, the rate of which can be limited by the diffusive separation rate of hydrogen across the homopause depending on the existing hydrogen mixing ratio (e.g., Walker, 1977), implies the rapid loss of hydrogen from early Earth and even possibly loss of entire water from Venus (e.g., Kasting and Pollack, 1983) under the enhanced EUV radiation emitted from the young Sun.

Early analytical studies of EUV-driven hydrodynamic escape investigated steady outflow solutions by solving simultaneous ordinary differential equations in the radial coordinate considering time derivatives to be zero in the conservation equations of mass, momentum and energy with spherical symmetry. This approach sometimes faces difficulty in finding transonic solutions to avoid mathematical singularity. Numerical time integration of conservation equations is a possible approach to resolve this problem.

By performing this calculation, Tian et al. (2005a) reported escape rates significantly lower than those estimated by earlier studies. Their calculation was performed at a temperature as low as 250 K at the base of hydrogen-

dominated region, which is presumably possible by effective cooling from a radiatively active secondary species. The obtained low escape rates would be attributed to the conductive loss of EUV heating energy toward the cold atmospheric base. Equating an estimate of the volcanic hydrogen degassing rate with the calculated escape rates, it was proposed that the early Earth atmosphere would be hydrogen rich with an H_2 mixing ratio as high as near 30%, even at 2.5 Ga. This significantly differs from the earlier estimates predicting an H_2 mixing ratio less than ~ 0.1 vol% during the Archean era (e.g., Walker, 1978).

Tian et al.'s numerical model, however, requires further testing for accuracy. In another paper (Tian et al., 2005b), they mentioned that their model scheme may have a difficulty in satisfying the radial uniformity of mass flux integral (taken over a sphere concentric with Earth) in steadily expanding isothermal solutions. This violation of the law of conservation of mass especially emerges at low altitudes in simulations with low atmospheric temperatures.

To avoid numerical instability, Tian et al. (2005a,b) used the Lax–Friedrichs (LF) scheme, which introduces an artificial numerical diffusion (LeVeque, 1992; de Sterck et al., 2001). At low altitudes, the atmospheric density profile approximately follows hydrostatic equilibrium. At low atmospheric temperature, the density contrast between altitudes in the lower atmosphere becomes significant owing to the decrease in atmospheric scale height. If the LF scheme is applied to such a system, the artificial numerical diffusive flux, approximately equivalent to that by a diffusion process with diffusivity given by the sound speed times the grid interval, may sometimes overwhelm the

true mass flux, particularly at low atmospheric altitudes. This calculation would thus cause a violation of the law of conservation of mass. On the other hand, calculated mass fluxes at the upper boundary are in good agreement with the analytical solution by Parker (1963), which is the main reason for using the LF scheme by Tian et al. (2005a,b).

It is still unclear whether the LF scheme adequately reproduces the escape rate even for non-isothermal atmosphere. At least, the problem with mass conservation in the lower altitudes implies significant errors in estimating energy balance in the outflow gas. Therefore, this study will simulate the EUV-driven hydrodynamic escape of hydrogen by using a more reliable numerical scheme.

We have developed a new numerical model that adopts the constrained interpolation profile (CIP) scheme (Yabe and Aoki, 1991; Yabe et al., 2001b), a high-accuracy method for solving advection equations. The advantage of the CIP scheme is that it causes few numerical dispersion errors by predicting the advection of both numerical values and their gradients at each grid point. Because of this nature and numerical stability, the CIP scheme is considered to be an adequate method to simulate atmospheric outflow.

2. Model

Following Tian et al. (2005a), the hydrodynamic flow of an ideal gas atmosphere composed of pure H₂ with radial symmetry is described by the inviscid Eulerian equations:

$$\frac{\partial(\rho r^2)}{\partial t} + \frac{\partial(\rho u r^2)}{\partial r} = 0, \quad (1)$$

$$\frac{\partial(\rho ur^2)}{\partial t} + \frac{\partial(\rho u^2 r^2 + pr^2)}{\partial r} = -\rho GM + 2pr, \quad (2)$$

$$\begin{aligned} \frac{\partial}{\partial t} \left[\left(\frac{\rho u^2}{2} + \frac{p}{\gamma - 1} \right) r^2 \right] + \frac{\partial}{\partial r} \left[\left(\frac{\rho u^2}{2} + \frac{\gamma p}{\gamma - 1} \right) ur^2 \right] = \\ -\rho u GM + qr^2 + \frac{\partial}{\partial r} \left(\kappa r^2 \frac{\partial T}{\partial r} \right), \end{aligned} \quad (3)$$

where r is the distance from the center, u is the radial velocity; ρ , p , T are the gas density, pressure, and temperature, respectively. γ is the ratio of specific heats considered as $7/5$, G is the gravitational constant, M is the mass of the Earth, κ is the thermal conductivity, and q is the heating rate. The equation of state is given by that of the ideal gas composed of pure H_2 . The thermal conductivity is given by

$$\kappa = \kappa_0 \left(\frac{T}{T_0} \right)^s, \quad (4)$$

where T_0 is the reference temperature, κ_0 is the thermal conductivity at $T = T_0$ and s is the constant power index. We set $T_0 = 250$ K, $\kappa_0 = 1.62 \times 10^{-1}$ J/m s K, and $s = 0.7$ (Hanley et al., 1970).

The heating rate q is calculated by the same method used by Tian et al. (2005a,b), which numerically solves the 2D radiative transfer of solar EUV flux incident from the solar direction into the spherically expanded atmosphere, and then laterally averages the energy absorption to obtain the radial heating profile at each time step. The EUV spectrum and the absorption cross section are provided by Woods and Rottman (2002) and Avakyan et al. (1998), respectively, for wavelengths shorter than 105 nm. To express the early solar EUV flux, the present-day time-averaged EUV spectrum is multiplied by enhancement factors neglecting the possible change in the spectrum profile. Furthermore, the heating efficiency of absorbed energy is considered

as 0.15 (Watson et al., 1981). The temperature at the lower boundary is fixed at 250 K. Each of these settings is basically the same as those used by Tian et al. (2005a).

Equations (1)–(3) are solved by explicit integration about time until the physical quantities settle into steady profiles. To perform time integration, we employ CIP schemes that are known to perform stable numerical integration of advection terms with a high degree of accuracy using reasonable computational resources. We adopted the CIP-CSL2 scheme (Yabe et al., 2001a) to solve the mass conservation equation because this method is optimized to guarantee the conservation of mass. To save computational resources, the original CIP scheme (Yabe and Aoki, 1991) is adopted for the advection terms of the momentum equation and the energy equation. The diffusion term in the energy equation is expressed by the centered difference formula. The upper and lower boundaries are set at $r=25$ Earth radius (6.36×10^3 km) and $r = 6.46 \times 10^3$ km (the Earth radius + 100 km), respectively. The interval was divided into 1000 numerical grids with the grid-to-grid intervals exponentially increasing with r .

In each simulation run, the atmospheric density and temperature at the lower boundary are fixed as a parameter as well as the EUV enhancement factor. The other physical quantities in the lower and upper boundaries are estimated by linear extrapolations from the calculated domain. The initial density profile is given by the isothermal hydrostatic structure for the lower layer and is proportional to r^{-2} in the upper layer beyond an arbitrary radius. A constant velocity of 10^{-5} m/s is set as the initial velocity profile.

3. Results

3.1. Testing isothermal calculation

To test the performance of our model, we simulated the steady expansion of the isothermal atmosphere into the vacuum and compared it with the analytical solution. This outflow is characterized by the escape parameter (Parker, 1963) defined as $\lambda_0 = GMm/kTr_0$ where m is the mass of an atmospheric molecule, k is the Boltzmann constant, and r_0 is the distance between the planetary center and the lower boundary of the atmosphere. Figure 1 shows the comparison between the analytical solutions and the numerical ones with various escape parameters. The solutions appear to match quite well.

We also carried out isothermal simulations with different total grid numbers. As shown in Figure 2, the calculated mass flux integrals approach the analytical ones with errors less than 2% as the total grid number increases up to 1000.

3.2. Full simulation results

Typical steady state solutions obtained by our full simulation, i.e., the numerical integration of the conservation equations of mass, momentum, and energy, are shown in Figure 3. For the solutions shown in Figures 3a, 3b, and 3c, we set the enhancement factor of solar EUV at unity and set several values of the gas density at the lower boundary. In each solution, the flow is radially accelerated from near zero velocity to supersonic, with the temperature profile peaking in the subsonic region.

In contrast to the results of Tian et al. (2005a), we obtained temperature profiles that did not approach constant temperature but continued to decrease at large distances from the center. This is due to the adiabatic cooling of expanding gas, which was also reproduced in earlier analytical studies (Sekiya et al., 1980; Watson et al., 1981). The approach to the isothermal profile observed by Tian et al. (2005a) may be caused by the lower gas density at great radial distances accompanied by a low outflow rate. In such a thin atmosphere, the thermal conduction may become very efficient to smooth out the temperature gradient.

Steady state solutions set at higher enhancement factors of solar EUV are shown in Figures 3d, 3e, and 3f, where the gas density at the lower boundary is maintained at $5 \times 10^{18} \text{ m}^{-3}$ for comparison. As the enhancement factor increases, the flow more strongly accelerates along with an increase in the temperature of the outflow gas. The temperature peak shifts upward with an enhanced EUV flux because the zone where EUV absorption occurs is pushed outward in the hotter, expanded atmosphere.

To confirm the reproducibility of energy conservation in our model, we compared the net energy outflow rate E_{out} with the net EUV heating rate E_{in} as follows:

$$E_{out} = 4\pi\rho_{top}r_{top}^2u_{top}(H_{top} - H_0) - 4\pi\left(\kappa r^2\frac{\partial T}{\partial r}\right)_{top} + 4\pi\left(\kappa r^2\frac{\partial T}{\partial r}\right)_0 \quad (5)$$

$$E_{in} = 4\pi\int_{r_0}^{r_{top}}qr^2dr \quad (6)$$

where the suffixes indicate the quantities estimated at the lower boundary (0) and the upper one (top), respectively, and H is the specific total energy of fluid given by the sum of the mechanical energy and enthalpy per unit

mass given by

$$H = \frac{1}{2}u^2 + \frac{\gamma}{\gamma - 1} \frac{P}{\rho} - \frac{GM}{r}. \quad (7)$$

In Figure 4, the ratios of E_{out}/E_{in} are shown for steady state numerical solutions. If the law of conservation of energy is satisfied, this ratio should be unity. For a given range of the EUV enhancement factor and the density at the lower boundary, the obtained E_{out}/E_{in} ratios are almost equal to unity with a relative error less than 3%. This indicates that our complete simulation preserves the law of conservation of energy very well.

In most of the steady numerical solutions, EUV heating energy is effectively transferred to mechanical energy. When we analyze the net energy outflow rate, the term of the flow flux of fluid energy predominates compared to the terms of thermal conduction across the upper and lower boundaries, irrespective of the EUV enhancement factor, as shown in Figure 5. Furthermore, the specific energy of fluid is dominated by mechanical energy rather than internal energy since the gas temperature is not high at the upper boundary. Therefore, more than half of EUV heating energy is transferred to the acceleration of escaping fluid, at least for the settings in Figure 5, implying that the solar EUV heating induces the effective escape of hydrogen.

4. Discussion

4.1. Escape rate of hydrogen

Our numerical results suggest that there is an effective loss of hydrogen from the early Earth atmosphere. In Figure 6, the hydrogen escape rate is shown as a function of the homopause hydrogen mixing ratio, which is converted from the lower boundary gas density. The conversion is carried

out by considering the diffusive separation of gas species in the layer above the homopause (see Appendix for details). Compared with the solutions obtained by Tian et al. (2005a), our numerical solutions yielded escape rates greater than several to several tens of factors, at the same hydrogen mixing ratios and EUV enhancement factors.

At a fixed EUV enhancement factor, we obtained escape rates that increase with the homopause hydrogen mixing ratio. When the mixing ratio, or the basal hydrogen density, is sufficiently high, the solar EUV is mostly absorbed in the atmospheric zone sufficiently far above the lower boundary. In such cases, the escape rate may gradually increase along with the basal hydrogen density. This is due to the expansion of the effective cross section of the whole Earth for the solar EUV radiation associated with the thickening of the atmosphere. However, when the basal hydrogen density is low, EUV may penetrate below the lower boundary. This suppresses the amount of EUV absorption heating in the calculated domain, resulting in a drop in the escape rate at low homopause hydrogen mixing ratios.

Our obtained escape rate is almost consistent with an order estimate, indicating that heating due to the solar EUV radiation accepted by the cross section of the solid Earth is fully transferred to the potential energy of the escaping gas, stated as follows:

$$\phi = \frac{\epsilon F_{EUV}}{4GM\mu/R_0} = 3.9 \times 10^{15} \left(\frac{\epsilon}{0.15} \right) \left(\frac{F_{EUV}}{F_{EUV,0}} \right) \text{ molecules/m}^2\text{s} \quad (8)$$

where F_{EUV} is the solar EUV flux integrated about wavelength, $F_{EUV,0}$ is its present mean value $6.9 \times 10^{-3} \text{ W/m}^2$, and ϵ is the heating efficiency of the absorbed EUV set at 0.15 in our simulations. This crude estimate closely follows the escape rates obtained at high basal hydrogen densities

(Figure 6). The difference of a factor can be explained by the partitioning of heating energy to kinetic energy of the escaping gas and less significantly to the conductive loss.

The relationship between the homopause mixing hydrogen ratio and escape rate asymptotically approaches the diffusion-limited flux as the EUV flux increases, as shown in Figure 6. This is reasonable behavior because the upward transport is regulated by the diffusion process across a layer that lies under the region where outflow acceleration begins. Note that the diffusion-limited flux defines the envelope of the maximum rate of diffusive separation of hydrogen molecules through the background stationary gas, which is composed of heavy species.

The realistic temperature of the upper atmosphere on early Earth remains under debate (e.g., Catling, 2006; Tian et al., 2006). If a higher temperature, as suggested from recent modeling studies (e.g., Lammer et al., 2009, and references therein), is considered at the lower boundary, the escape rate increases expectedly. When the lower boundary density is fixed, the lower boundary pressure increases with temperature. This is equivalent to the increase in the column density of hydrogen, resulting in efficient EUV absorption above the lower boundary.

4.2. Level of hydrogen in early Earth atmosphere

From the Earth's atmosphere today, hydrogen escapes at a rate of approximately $1\text{--}1.5 \times 10^{12}$ H₂ molecules /m² s (Hunten and Donahue, 1976). For convenience, we use a value equivalent to the H₂ flux because hydrogen takes various chemical forms during its upward transport. A recent estimate of the current volcanic outgassing rate of hydrogen is $1.8 \pm 1.3 \times 10^{14}$ H₂

molecules/m² s (Holland, 2002; Martin et al., 2007), although much lower estimates on the order of 10¹² H₂ molecules/m² s are also found in earlier literature (e.g., Walker, 1977; Kasting and Donahue, 1981). An uncertainty in these estimates is the volcanic outgassing rate of water vapor, from which the hydrogen outgassing rate is deduced that provides a typical H₂/H₂O ratio of volcanic gas. If a recent estimate is adopted, there should be some sink of H₂ on Earth because the outgassing rate is greater than the escape rate. In the oxidized Earth atmosphere of today, the oxidation of hydrogen through the photochemical reaction is most likely to be the major removal mechanism of free hydrogen (e.g., Walker, 1978).

During the Archean era (2.5–4.0 Ga), the atmospheric hydrogen level might have been substantially determined by the balance between the outgassing rate and the rate of escape because of the low oxygen level in the atmosphere. On the basis of the compilation of sedimentary rock records that indicate a constraint to the oxidation state of the surface environment, it is widely accepted that the Earth’s atmosphere was anoxic before 2.45 Ga (e.g., Canfield, 2005; Holland, 2006). In such an anoxic atmosphere, the rate of removal of H₂ by photochemical oxidation would be negligible. Therefore, we assume that the atmospheric hydrogen level was regulated by the balance between the rates of outgassing and escape during the Archean era. It should, however, be considered that other chemical pathways to consume hydrogen, including the reduction of the oxidized outgas component such as SO₂ and biological fixation, would also have played an important role on early Earth (e.g., Holland, 2002; Rosing et al., 2010). If these processes work, they should lower the hydrogen level below that achieved by the balance between

outgassing and escape.

At the end of the Archean era, the solar EUV radiation was likely 2.5 times higher than the present flux (Ribas et al., 2005). At the same time, the volcanic H₂ outgassing flux may have been 5 times higher on the basis of thermal history model by Turcotte (1980), implying an outgassing flux 9×10^{14} H₂ molecules/m² s (Tian et al., 2005a). Setting these parameters, the balance of our obtained escape flux with the outgassing flux predicts a H₂ mixing ratio about 1.3 vol% at the homopause (Figure 6). This is smaller than the previous estimate (Tian et al., 2005a) by a factor of nearly 25, although still slightly higher than the estimate derived from the balance using the diffusion-limited flux. Figure 6 indicates that this value is weakly dependent on estimates of the outgassing rate of hydrogen but strongly dependent on the EUV enhancement factor.

As noted previously, the thermal state of the upper atmosphere of early Earth remains poorly constrained at 250 K, which we assume is a lower estimate for the base of the hydrogen-dominated layer. If a higher temperature is used at the base, the balancing H₂ mixing ratio should decrease because of more efficient escape. We therefore suggest that the H₂ mixing ratio at the homopause was likely below ~ 1 vol% in the early Earth atmosphere during the Archean era.

Rosing et al. (2010) proposed that the oxidation state of shallow marine Fe-bearing sediments may be used to constrain H₂ levels in the early Earth atmosphere. Assuming thermodynamic equilibrium, the widespread existence of Fe₃O₄ in Archean sediments implies that the corresponding H₂ level was $\sim 2 \times 10^{-2}$ atm at maximum, although the authors speculate that the actual

H₂ level might have been much lower than this value because of hydrogen consumption by methanogen biological activity. Rosing et al.'s mineralogical estimate seems fairly consistent with ours, whereas the assumption of thermodynamic equilibrium between the atmosphere and sedimentary minerals needs to be further verified (e.g., Reinhard and Planavsky, 2011).

The low H₂ level might also be consistent with mass independent fractionation (MIF) of sulfur isotopes found in Archean sedimentary rocks (Farquhar et al., 2000). The sulfur MIF records have been accepted as strong evidence for an anoxic Earth atmosphere (e.g., Pavlov and Kasting, 2002) on the basis of geochemical modeling. Currently, the models explaining sulfur MIF implicitly assume that the hydrogen content is kept low by diffusion-limited escape. Because MIF of sulfur was probably caused by photolysis of atmospheric SO₂ (Farquhar et al., 2000, 2001), the Archean atmosphere likely had oxidation states opening the reaction path of SO₂ photolysis. If the atmosphere was abundant in H₂, outgassed SO₂ would have been easily reduced to H₂S or other species leaving few MIF anomalies (Kasting and Howard, 2006). Therefore, the existence of a sulfur MIF signature might constrain the upper limit for the atmospheric hydrogen level. At present, sulfur chemistry in a H₂-rich atmosphere remains an open issue, and its further examination would be worthwhile to constrain the hydrogen content in the early Earth atmosphere.

It is to be noted that the H₂ level at the homopause does not necessarily represent the hydrogen level in the lowermost atmosphere. It may instead represent an approximate net abundance of hydrogen-bearing chemical species at the cold trap, such as H₂O and CH₄, because these species

release hydrogen by UV photolysis in the stratosphere unless UV is effectively shielded by other component(s). Therefore, our results imply that the Earth's atmosphere might have contained less than $\sim 1\text{vol}\%$ of equivalent H_2 as a hydrogen-bearing species during the Archean era. According to the recent calculation of the greenhouse effect in the early Earth's atmosphere (Haqq-Misra et al., 2008), atmospheric methane, an expected major species hosting hydrogen in the early atmosphere, may have helped to warm the Earth by $\sim 10\text{ K}$ in the mixing ratio from 10^{-3} to 10^{-2} . This may have helped to prevent global freezing of the early Earth under the faint Sun, but there is a need for other warming agent(s) to explain the high global temperature suggested by geological records (Haqq-Misra et al., 2008).

5. Conclusions

We have carried out numerical simulations of the hydrodynamic escape of hydrogen by adopting a high-accuracy scheme for solving the one-dimensional advection equation. According to our results, EUV heating energy is effectively converted to mechanical energy of the outflow gas in contrast to an earlier study that employed another numerical scheme. The obtained numerical solutions more adequately reproduce the escape flow because they satisfy the laws of conservation of mass and energy with a small error. Our result suggests that the homopause mixing ratio of hydrogen in the early Earth atmosphere was likely maintained lower than $\sim 1\text{ vol}\%$ during Archean even when the higher volcanic degassing rate of hydrogen was considered. This appears consistent with geological evidence implying low hydrogen content in the early Earth atmosphere.

Acknowledgements

We thank Ko-ichiro Sugiyama and EPnetFaN members for providing us computation environment and technical advice. We also thank anonymous reviewers for constructive comments. The physics of diffusive separation of gas species is significantly improved by the suggestion from a reviewer. This work was supported by MEXT KAKENHI Grant Number 23103003.

Appendix: Estimation of homopause hydrogen mixing ratio

The homopause hydrogen mixing ratio is estimated for a two-component atmosphere with the following assumptions: (1) The homopause is located below the altitude of the lower boundary of outflow calculation. (2) Between the homopause and the lower boundary, the atmosphere is isothermal (at 250 K), and the diffusive separation of H₂ through background heavy gas occurs. (3) The heavy species has no vertical flux. (4) At the lower boundary, H₂ is dominant: the volume mixing ratio of H₂:heavy species is 10:1. (5) The homopause density is maintained at a characteristic constant value independent of the hydrogen flow. These assumptions follow those of Tian et al. (2005a) except in the detail of assumption (2), in which the effects of the H₂ diffusive flux on the gas density profile were not considered. These effects are considered in our study.

Subscripts 1 and 2 denote the physical quantities of light species and heavy ones, respectively. Following Hunten (1973) and given the above assumptions, the diffusion equations for both species having a vertical velocity w_i are:

$$w_1 - w_2 = -\frac{b_{12}}{n_2} \left(\frac{1}{n_1} \frac{dn_1}{dz} + \frac{m_1 g}{kT} \right) \quad (A1)$$

$$w_2 - w_1 = -\frac{b_{12}}{n_1} \left(\frac{1}{n_2} \frac{dn_2}{dz} + \frac{m_2 g}{kT} \right) \quad (\text{A2})$$

where g is the gravity, b_{12} is the binary diffusion coefficient, n_i is the number density, and z is the altitude.

When the heavy species remains stationary, i.e., $w_2 = 0$, equation (A1) may be modified by using the upward flux of light species, $\phi_1 = n_1 w_1$:

$$\phi_1 = -b_{12} f_1 \left(\frac{1}{f_1} \frac{df_1}{dz} + \frac{1}{n_2} \frac{dn_2}{dz} + \frac{m_1 g}{kT} \right) \quad (\text{A3})$$

where $f_1 = n_1/n_2$. From equation (A2), the distribution of n_2 is expressed by

$$\frac{1}{n_2} \frac{dn_2}{dz} = -\frac{1}{H_2} \quad (\text{A4})$$

where

$$H_2 = \left(\frac{m_2 g}{kT} - \frac{\phi_1}{b_{12}} \right)^{-1}. \quad (\text{A5})$$

This formula indicates that the upward flux of light species has an effect of stretching the scale height, H_2 , of heavy species. Substituting equation (A4) in (A3), the distribution of light species relative to the heavy one is expressed as:

$$\frac{df_1}{dz} = -\frac{\phi_1(1 + f_1) + \frac{(m_1 - m_2)gb_{12}}{kT} f_1}{b_{12}}. \quad (\text{A6})$$

Then,

$$f_1(z) = c + (f_1(z_0) - c) \exp \left\{ \frac{z - z_0}{H_{12}} \right\} \quad (\text{A7})$$

where z_0 is the reference altitude and

$$H_{12} = \left(\frac{(m_2 - m_1)g}{kT} - \frac{\phi_1}{b_{12}} \right)^{-1}, \quad c = \frac{\phi_1 H_{12}}{b_{12}}. \quad (\text{A8})$$

From equation (A4),

$$n_2(z) = n_2(z_0) \exp \left\{ -\frac{z - z_0}{H_2} \right\}. \quad (\text{A9})$$

Considering species 1 and 2 to be H₂ and N₂, respectively, the homopause hydrogen mixing ratio is estimated by the following procedure. First, z_0 is set to be the altitude of the lower boundary of outflow calculation, then we substitute the lower boundary hydrogen density to $n_1(z_0)$, $f_1(z_0) = 10$, and the hydrogen outflow rate to ϕ_1 in equations (A7) and (A9). Here $b_{12} = 1.71 \times 10^{21} \text{ m}^{-1} \text{ s}^{-1}$ at $T=250 \text{ K}$ (Hunten, 1973) and $g = 9.5 \text{ m/s}^2$ considering the layer to be $\sim 100 \text{ km}$ above the Earth's surface. Second, the homopause altitude $z = z_h$ (in practice, the difference $z_h - z_0$) is numerically obtained so as to satisfy $n_1(z_h) + n_2(z_h) = (f_1(z_h) + 1)n_2(z_h) = n_{homo}$, where the homopause gas density n_{homo} is considered to be 10^{19} m^{-3} (Tian et al., 2005a). The homopause hydrogen mixing ratio, x_1 , is then obtained as $x_1 = f_1(z_h)/(1 + f_1(z_h))$.

Note that Tian et al. (2005a) neglected the effects of the upward flux of hydrogen. This approximation may not be a serious error when the hydrogen flux is as small as they have estimated, but it is inappropriate to apply to our simulation runs. Because we found that the upward hydrogen flux has an effect of stretching the scale height of the heavy species, the homopause hydrogen mixing ratio becomes larger when this effect is considered.

By taking $\frac{df_1}{dz} \rightarrow 0$ from equation (A6), the diffusion-limited escape flux of light species is acquired as

$$\phi_{1,lim} = \frac{(m_2 - m_1)gb_{12}x_1}{kT}. \quad (\text{A10})$$

This implies that the limiting flux is achieved when vertical fractionation between gas species is minimal. In Figure 6, our obtained flux is always lower than the limiting flux for each homopause mixing ratio. This is consistent with our assumption that the hydrogen upward transport obeys the diffu-

sion process before reaching the high altitude region where hydrodynamic acceleration occurs.

References

- Avakyan, S. V., Ii'In, R. N., Lavrov, V. M., Ogurtsov, G. N., 1998. Collision processes and excitation of UV emission from planetary atmospheric gases: A handbook of cross sections. Gordon and Breach Science Publishers, Amsterdam.
- Canfield, D. E., 2005. The early history of atmospheric oxygen: homage to Robert M. Garrels. *Annu. Rev. Earth Planet. Sci.* 33, 1–36.
- Catling, D. C., 2006. Comment on “a hydrogen-rich early Earth atmosphere”. *Science* 311, 38–38.
- de Sterck, H., Abeele, D. V., Poedts, S., Deconinck, H., et al., 2001. Stationary two-dimensional magnetohydrodynamic flows with shocks: characteristic analysis and grid convergence study. *J. Comput. Phys.* 166, 28–62.
- Farquhar, J., Bao, H., Thiemens, M. H., 2000. Atmospheric influence of Earth's earliest sulfur cycle. *Science* 289 (5480), 756–758.
- Farquhar, J., Savarino, J., Airieau, S., Thiemens, M. H., 2001. Observation of wavelength-sensitive mass-independent sulfur isotope effects during SO₂ photolysis: Implications for the early atmosphere. *J. Geophys. Res.* 106, 32829–32832.

- Hanley, H. J. M., Intemann, H., McCarty, R. D., 1970. The viscosity and thermal conductivity of dilute gaseous hydrogen from 15 to 5000 k. *J. Res. Nat. Bur. Stand. Sect. A* 74, 331–353.
- Haqq-Misra, J. D., Domagal-Goldman, S. D., Kasting, P. J., Kasting, J. F., 2008. A revised, hazy methane greenhouse for the Archean Earth. *Astrobiol.* 8, 1127–1137.
- Holland, H. D., 2002. Volcanic gases, black smokers, and the great oxidation event. *Geochim. Cosmochim. Acta* 66, 3811–3826.
- Holland, H. D., 2006. The oxygenation of the atmosphere and oceans. *Phil. Trans. Royal Soc. B: Bio. Sci.* 361, 903–915.
- Hunten, D. M., 1973. The escape of light gases from planetary atmospheres. *J. Atmos. Sci.* 30, 1481–1494.
- Hunten, D. M., Donahue, T. M., 1976. Hydrogen loss from the terrestrial planets. *Ann. Rev. Earth Planet. Sci.* 4, 265–292.
- Kasting, J. F., Donahue, T. M., 1981. Evolution of oxygen and ozone in Earths atmosphere. In: *Life in the Universe*. Vol. 1. pp. 149–162.
- Kasting, J. F., Howard, M. T., 2006. Atmospheric composition and climate on the early Earth. *Phil. Trans. Royal Soc. B: Bio. Sci.* 361 (1474), 1733–1742.
- Kasting, J. F., Pollack, J. B., 1983. Loss of water from Venus. I. Hydrodynamic escape of hydrogen. *Icarus* 53, 479–508.

- Lammer, H., Kasting, J. F., Chassefière, E., Johnson, R. E., Kulikov, Y. N., Tian, F., 2009. Atmospheric escape and evolution of terrestrial planets and satellites. *Space Sci. Rev.* 139, 399–436.
- LeVeque, R. J., 1992. Numerical methods for conservation laws. Birkhäuser, Berlin.
- Martin, R. S., Mather, T. A., Pyle, D. M., 2007. Volcanic emissions and the early Earth atmosphere. *Geochim. Cosmochim. Acta* 71, 3673–3685.
- Parker, E. N., 1963. Interplanetary dynamical processes. Interscience Publishers, New York.
- Pavlov, A. A., Kasting, J. F., 2002. Mass-independent fractionation of sulfur isotopes in Archean sediments: strong evidence for an anoxic Archean atmosphere. *Astrobiology* 2 (1), 27–41.
- Reinhard, C. T., Planavsky, N. J., 2011. Mineralogical constraints on Precambrian $p\text{CO}_2$. *Nature* 474, E1–E1.
- Ribas, I., Guinan, E. F., Güdel, M., Audard, M., 2005. Evolution of the solar activity over time and effects on planetary atmospheres. I. High-energy irradiances (1–1700 Å). *Astrophys. J.* 622, 680–694.
- Rosing, M. T., Bird, D. K., Sleep, N. H., Bjerrum, C. J., 2010. No climate paradox under the faint early Sun. *Nature* 464, 744–747.
- Sekiya, M., Nakazawa, K., Hayashi, C., 1980. Dissipation of the primordial terrestrial atmosphere due to irradiation of the solar EUV. *Prog. Theor. Phys.* 64, 1968–1985.

- Tian, F., Toon, O. B., Pavlov, A. A., 2006. Response to comment on “a hydrogen-rich early Earth atmosphere”. *Science* 311, 38–38.
- Tian, F., Toon, O. B., Pavlov, A. A., de Sterck, H., 2005a. A hydrogen-rich early Earth atmosphere. *Science* 308, 1014–1017.
- Tian, F., Toon, O. B., Pavlov, A. A., de Sterck, H., 2005b. Transonic hydrodynamic escape of hydrogen from extrasolar planetary atmospheres. *Astrophys. J.* 621, 1049–1060.
- Turcotte, D. L., 1980. On the thermal evolution of the Earth. *Earth Planet. Sci. Lett.* 48, 53–58.
- Walker, J. C. G., 1977. *Evolution of the Atmosphere*. Macmillan and Collier Macmillan, New York and London.
- Walker, J. C. G., 1978. Oxygen and hydrogen in the primitive atmosphere. *Pure Appl. Geophys.* 116, 222–231.
- Watson, A. J., Donahue, T. M., Walker, J. C. G., 1981. The dynamics of a rapidly escaping atmosphere: Applications to the evolution of Earth and Venus. *Icarus* 48, 150–166.
- Woods, T. N., Rottman, G. J., 2002. Solar ultraviolet variability over time periods of aeronomic interest. In: *Geophysical Monograph 130*. American Geophysical Union, Washington, D.C., pp. 221–234.
- Yabe, T., Aoki, T., 1991. A universal solver for hyperbolic equations by cubic-polynomial interpolation i. one-dimensional solver. *Comput. Phys. Commun.* 66, 219–232.

- Yabe, T., Tanaka, R., Nakamura, T., Xiao, F., 2001a. An exactly conservative semi-lagrangian scheme (CIP-CSL) in one dimension. *Mon. Weather Rev.* 129, 332–344.
- Yabe, T., Xiao, F., Utsumi, T., 2001b. The constrained interpolation profile method for multiphase analysis. *J. Comput. Phys.* 169, 556–593.

Figure Captions

Figure 1 Comparison of analytical solutions and numerical ones for the isothermal steady expansion of the atmosphere. Radial density (top panel) and velocity profiles (lower panel) are scaled by the basal density and sound velocity, respectively. Independent of the escape parameter over this range (taken at 5, 15, and 25), the numerical solutions are indistinguishable from the analytical ones.

Figure 2 Relative differences between mass fluxes obtained from numerical calculations and analytical solutions for the isothermal steady expansion of the atmosphere. When we increase grid numbers to 1000, the difference becomes less than 2% for escape parameters 5, 15, and 25.

Figure 3 Steady state solutions obtained by full numerical simulations. The left and right columns show dependence on the hydrogen density at the lower boundary and on the EUV flux, respectively. For each profile, the plus mark represents the sonic point. In the panels of the velocity profile, the escape velocity is also shown.

Figure 4 Ratios of the net energy outflow rate and net heating rate for the steady numerical solutions.

Figure 5 Analysis of the energy outgoing rate. The total (square) is divided into the term of the flow flux of fluid energy (plus) and the heat flow terms due to the thermal conduction at the upper boundary (cross) and lower one (star). In this calculation, the hydrogen number density is considered to be $5 \times 10^{18} \text{ m}^{-3}$ at the lower boundary.

Figure 6 Hydrogen escape rate as a function of the homopause hydrogen

mixing ratio. Numerical solutions at EUV enhancement factors 1, 2.5, 5, and 10 are shown in each solid curve, which shows escape rates significantly larger than those obtained by the previous study (Tian et al., 2005a, dashed curves). Volcanic outgassing rates of hydrogen estimated for the modern Earth mantle 1.8×10^{14} H₂ molecules/m² (Holland, 2002) and the Archean one (5 times the present, Turcotte, 1980) are also shown by the horizontal lines. A comparison of the diffusion-limited escape flux is also shown here.

Figure 1.

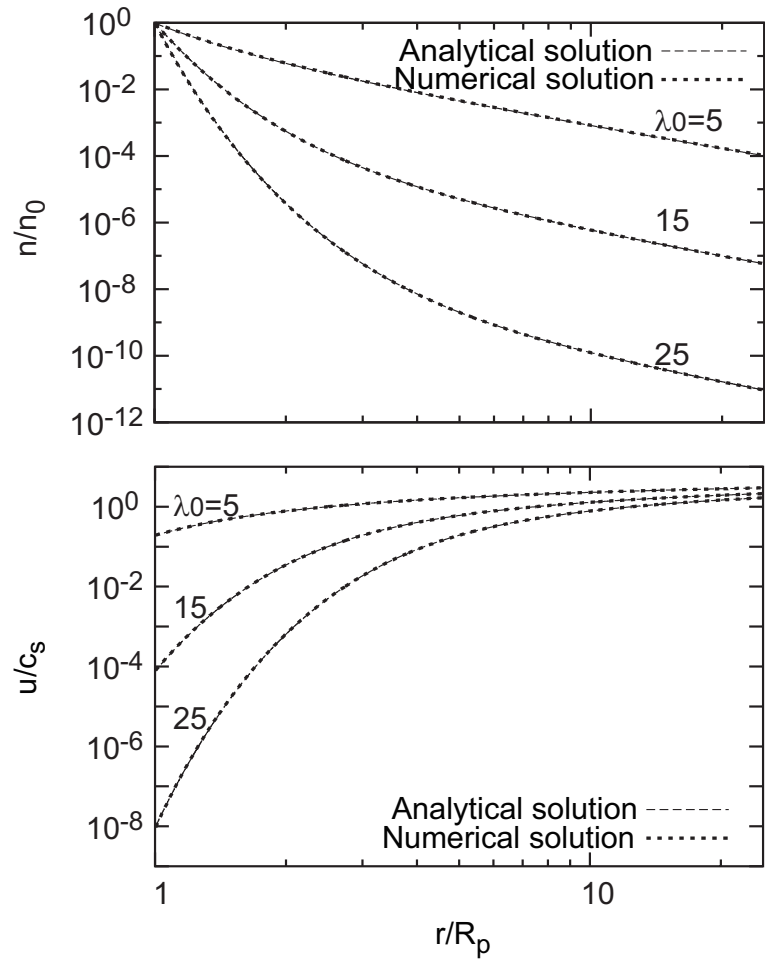


Figure 2.

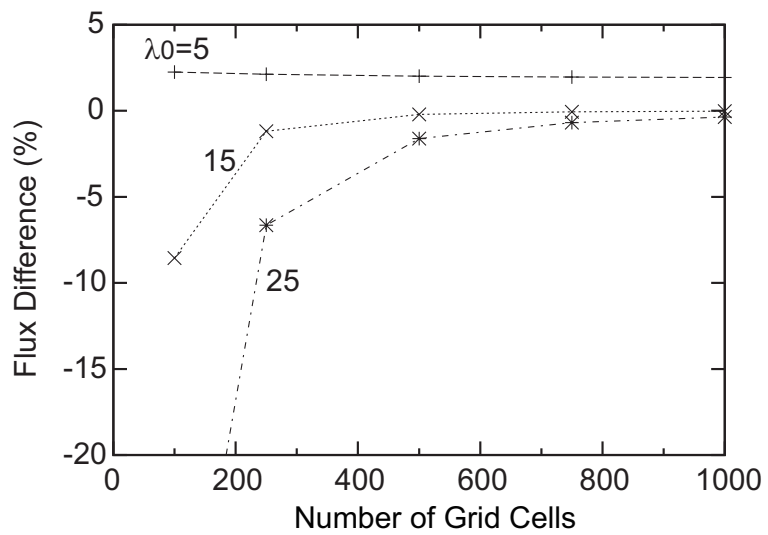


Figure 3.

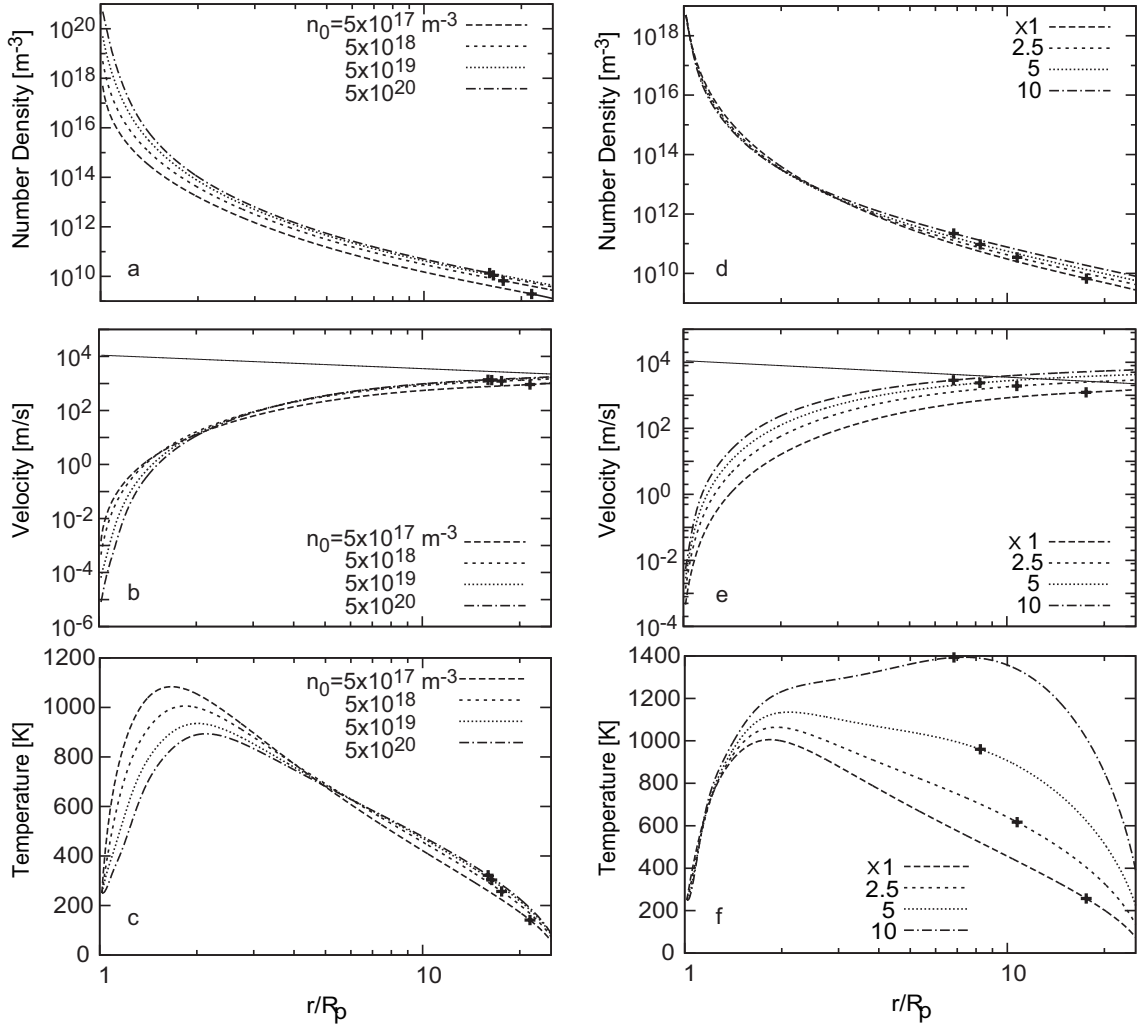


Figure 4.

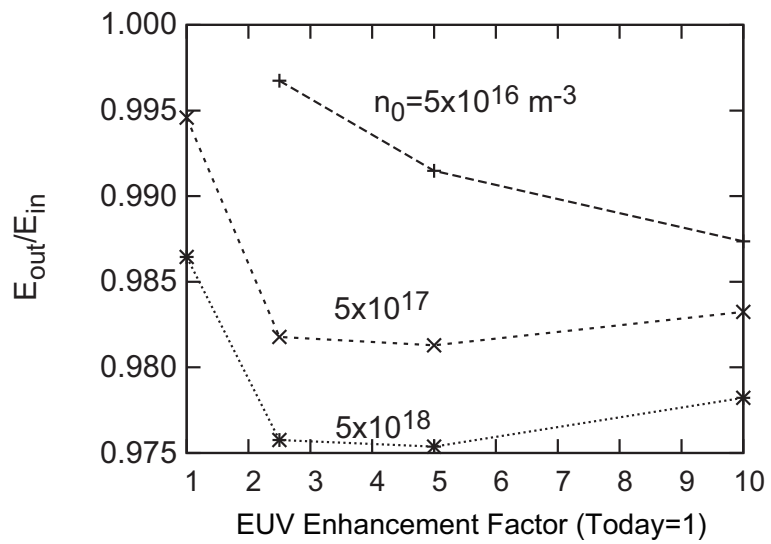


Figure 5.

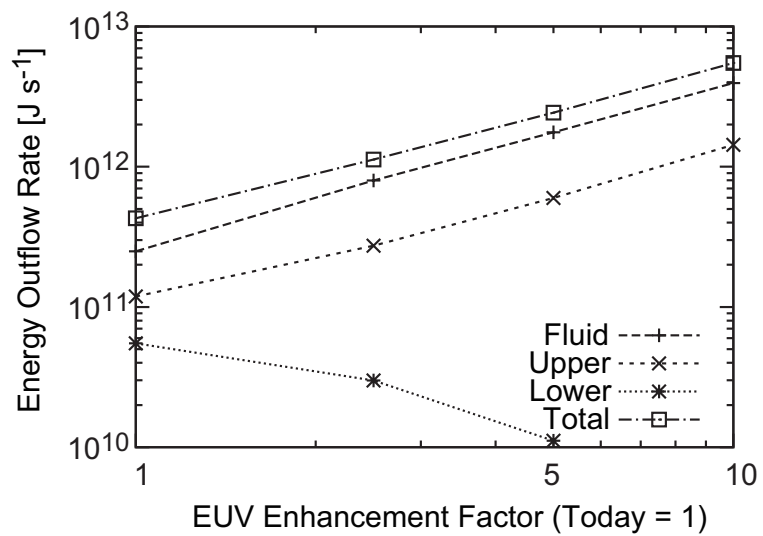


Figure 6.

